RESEARCH ARTICLE

Pharmacological inhibition of TRPV2 attenuates phagocytosis and lipopolysaccharide-induced migration of primary macrophages

Rick Raudszus[1] | Andrea Paulig[1] | Nicole Urban[1] | Anke Deckers[2] |
Simone Gräßle[2] | Sylvia Vanderheiden[2] | Nicole Jung[2] | Stefan Bräse[2,3] |
Michael Schaefer[1] | Kerstin Hill[1]

[1]Rudolf-Boehm-Institute of Pharmacology and Toxicology, Leipzig University, Leipzig, Germany

[2]Institute of Biological and Chemical Systems, Karlsruhe Institute of Technology, Karlsruhe, Germany

[3]Institute of Organic Chemistry, Karlsruhe Institute of Technology, Karlsruhe, Germany

Correspondence
Kerstin Hill, Rudolf-Boehm-Institute of Pharmacology and Toxicology, Leipzig University, Leipzig, Germany.
Email: kerstin.hill@medizin.uni-leipzig.de

Abstract

Background and Purpose: In macrophages, transient receptor potential vanilloid 2 (TRPV2) channel contributes to various cellular processes such as cytokine production, differentiation, phagocytosis and migration. Due to a lack of selective pharmacological tools, its function in immunological processes is not well understood and the identification of novel and selective TRPV2 modulators is highly desirable.

Experimental Approach: Novel and selective TRPV2 modulators were identified by screening a compound library using Ca^{2+} influx assays with human embryonic kidney 293 (HEK293) cells heterologously expressing rat TRPV2. Hits were further characterized and validated with Ca^{2+} influx and electrophysiological assays. Phagocytosis and migration of macrophages were analysed and the contribution of TRPV2 to the generation of Ca^{2+} microdomains was studied by total internal reflection fluorescence microscopy (TIRFM).

Key Results: The compound IV2-1, a dithiolane derivative (1,3-dithiolan-2-ylidene)-4-methyl-5-phenylpentan-2-one), is a potent inhibitor of heterologously expressed TRPV2 channels ($IC_{50} = 6.3 \pm 0.7$ μM) but does not modify TRPV1, TRPV3 or TRPV4 channels. IV2-1 also inhibits TRPV2-mediated Ca^{2+} influx in macrophages. IV2-1 inhibits macrophage phagocytosis along with valdecoxib and after siRNA-mediated knockdown. Moreover, TRPV2 inhibition inhibits lipopolysaccharide-induced migration of macrophages whereas TRPV2 activation promotes migration. After activation, TRPV2 shapes Ca^{2+} microdomains predominantly at the margin of macrophages, which are important cellular regions to promote phagocytosis and migration.

Conclusions and Implications: IV2-1 is a novel TRPV2-selective blocker and underline the role of TRPV2 in macrophage-mediated phagocytosis and migration. Furthermore, we provide evidence that TRPV2 activation generates Ca^{2+} microdomains, which may be involved in phagocytosis and migration of macrophages.

Abbreviations: BMDM, bone marrow-derived macrophages; IV2-1, inhibitor 5-(1,3-dithiolan-2-ylidene)-4-methyl-5-phenylpentan-2-one; IV2-2, inhibitor 4-[1,3-dithiolan-2-ylidene(phenyl)methyl]-5-methylhexan-2-one; IV2-3, inhibitor 5-(1,3-dithiolan-2-ylidene)-4-methyl-5-phenyl-pentan-2-ol.

1 | INTRODUCTION

In recent decades, academic drug discovery enormously benefited from progresses in automation combined with complex computational support. Widely used in life science and pharmaceutical industry, even specialized assays can now be scaled up to medium- or high-throughput screening (HTS) generating more data in less time. Among other fields of experimental pharmacology, this led, for instance, to the identification of many new ion channel modulators. **Transient receptor potential (TRP) channels** form a superfamily of mainly non-selective cation channels, which are involved in a variety of physiological and pathophysiological processes, such as nociception or thermosensation. They are affected by various chemical and physical stimuli (Nilius & Owsianik, 2011). Nevertheless, besides well-investigated members such as **TRP vanilloid 1 (TRPV1)** (Bevan et al., 2014; Jara-Oseguera et al., 2008), there are several channels such as **TRPV2**, whose physiological and pathophysiological roles are not very well understood.

TRPV2 is a Ca^{2+}-permeable cation channel that is highly expressed in cells of the adaptive and innate immune system (Entin-Meer & Keren, 2020; Froghi et al., 2021; Santoni et al., 2013). Previously published reports provide evidence that TRPV2 contributes to migration in neutrophils, degranulation in mast cells, T-cell receptors and Ca^{2+} signalling in T-cells (Heiner et al., 2003; Sauer & Jegla, 2006; Zhang et al., 2012). In macrophages, TRPV2 is associated with cytokine production, differentiation, phagocytosis and migration (Iwata et al., 2020; Kajiya et al., 2010; Link et al., 2010; Nagasawa et al., 2007; Yamashiro et al., 2010), and cellular processes that are indispensable for innate immunity. In this context, Link et al. (2010) previously demonstrated that TRPV2-deficient mice showed a reduced bacterial clearance and accelerated mortality after a *Listeria monocytogenes* infection. Moreover, TRPV2-deficient peritoneal macrophages (PM) exhibited reduced basal and chemoattractant-mediated motility, impaired particle binding and attenuated phagocytosis (Link et al., 2010). TRPV2 is supposed to be recruited to nascent phagosomes that initiate depolarization or to be involved in the first steps of pseudopodia and podosome assembly (Entin-Meer & Keren, 2020; Koyasu, 2010; Link et al., 2010; Yamashiro et al., 2010). However, experiments using a genetic knockout or knockdown approach may also cause genetic compensation mechanisms that may affect cellular phenotypes. Small molecules that acutely modulate TRPV2 function might therefore, further elucidate the role of TRPV2 in immunological processes. Due to the lack of selective TRPV2 activators and the sparse availability of selective and potent TRPV2 inhibitors, most studies are based on unselective TRPV2 modulators. TRPV2 activators **2-aminoethoxydiphenyl borate (2-APB)** or **probenecid** are far from selective for TRPV2. The same applies to the broad TRP channel

What is already known

- TRPV2 is expressed in mouse macrophages and contributes to macrophage phagocytosis and migration.

What does this study add

- Identification and characterization of the novel TRPV2 channel blocker 5-(1,3-dithiolan-2-ylidene)-4-methyl-5-phenylpentan-2-one (IV2-1).
- Acute modulation of TRPV2 by IV2-1 inhibits macrophage migration and phagocytosis.

What is the clinical significance

- TRPV2 might be a novel and promising target to treat immune disorders.

blocker **ruthenium red** (Colton & Zhu, 2007). Recently, **valdecoxib** has been described as a novel blocker of TRPV2 (Bluhm et al., 2022). Although the block by valdecoxib is selective for TRPV2 within the TRP channel family, valdecoxib also affects **cyclooxygenase-2 (COX-2),** which might interfere with assays investigating the role of TRPV2 in macrophage function.

Herein, we present 5-(1,3-dithiolan-2-ylidene)-4-methyl-5-phenylpentan-2-one (inhibitor V2-1; IV2-1), a novel TRPV2-selective blocker, which blocks TRPV2 activation by 2-APB or by an agonist combination of 2-APB and probenecid. Additionally, we demonstrate the functional expression of TRPV2 in primary bone marrow-derived macrophages (BMDM) from mice by blocking TRPV2-mediated Ca^{2+} influx with IV2-1 or small interfering RNA (siRNA). In macrophages, we observed a significant attenuation of phagocytosis and migration when TRPV2 was inhibited by IV2-1, valdecoxib and after siRNA-mediated knockdown. In contrast, TRPV2 activation with a combination of 2-APB and probenecid resulted in a promoted migration. In addition, total internal reflection fluorescence microscopy (TIRFM) revealed that TRPV2 activation shapes Ca^{2+} microdomains in macrophages predominantly located at the margin of the cells, which may directly affect phagocytosis or migration.

2 | METHODS

2.1 | Cell culture and isolation of primary macrophages

Human embryonic kidney 293 (HEK293) cell lines stably transfected with expression plasmids that encode cyan fluorescent protein (CFP)-tagged rat TRPV2 (HEK$_{TRPV2}$), cyan fluorescent protein-tagged rat TRPV1, cyan fluorescent protein-tagged mouse TRPV3 and yellow fluorescent protein (YFP)-tagged mouse TRPV4 were generated and maintained as previously described (Urban et al., 2012). Cell lines were cultured in Earle's minimum essential medium (MEM), supplemented with 10% foetal calf serum (FCS), 2 mM of L-glutamine, 100 units·ml^{-1} of penicillin, 0.1 mg·ml^{-1} of streptomycin and 0.6 mg·ml^{-1} of geneticin. HEK293 cells as control group were cultured in Earle's minimum essential medium, supplemented with 10% foetal calf serum, 2 mM of L-glutamine, 100 units·ml^{-1} of penicillin and 0.1 mg·ml^{-1} of streptomycin. For single-cell [Ca^{2+}]$_i$ imaging and electrophysiological experiments, HEK$_{TRPV2}$ cells were plated onto 25-mm glass coverslips (coated with poly-L-lysine for HEK293 cells) and measured 24–48 h after seeding. All cells were maintained at 37°C in a 5% CO$_2$-aerated, humidified atmosphere.

In contrast to cell lines, using primary cells from mice to study physiological mechanisms helps to improve reliability of the results. For several decades, C57BL/6 mice are used to investigate immunological processes or cancer (Song & Hwang, 2017). Therefore, primary BMDM or peritoneal macrophages were obtained from C57BL/6 mice at 2–3 months of age as described previously by Zhang et al. (2008). Animal studies are reported in compliance with the ARRIVE guidelines (Percie du Sert et al., 2020) and with the recommendations made by the *British Journal of Pharmacology* (Lilley et al., 2020). Experiments including mice or cells derived from mice were approved by the local authorities (Landesdirektion Leipzig [Regional office Saxony], Reference No. DD24-5131/347/7) and performed according to the European (Council Directive 2010/63/EU) and German guidelines for the welfare of experimental animals. Mice were killed by cervical dislocation. All conceivable efforts were taken to replace, reduce and refine animal experiments. Cells were cultured in Iscove's modified Dulbecco's medium (IMDM), supplemented with 10% foetal calf serum, 2 mM of L-glutamine, 100 units·ml^{-1} of penicillin, 0.1 mg·ml^{-1} of streptomycin, 20 ng·ml^{-1} of recombinant murine **macrophage colony-stimulating factor (M-CSF)** (Wagner et al., 2014) and 50 μM of 2-mercaptoethanol at 37°C in a 5% CO$_2$-aerated, humidified atmosphere. Adherent BMDM were harvested by washing 3 times with cold 0.8 mM of ethylenediaminetetraacetic acid (EDTA)-containing phosphate-buffered saline (PBS), 1 time with cold EDTA-free PBS and gentle pipetting with media. For single-cell [Ca^{2+}]$_i$ imaging, BMDM were plated or grown onto 25-mm glass coverslips. BMDM were polarized with 100 ng·ml^{-1} of **lipopolysaccharide (LPS)** and 10 ng·ml^{-1} of **interferon γ (IFN-γ)** for 24 h in growth medium before experiments. The immuno-related procedures used comply with the recommendations made by the *British Journal of Pharmacology* (Alexander et al., 2018).

2.2 | Fluorometric [Ca^{2+}]$_i$ imaging

All fluorometric Ca^{2+} assays were conducted in 4-(2-hydroxyethyl)-1-piperazineethanesulfonic acid (HEPES)-buffered saline, which contained 132 mM of NaCl, 6 mM of KCl, 1 mM of MgCl$_2$, 1 mM of CaCl$_2$, 5.5 mM of glucose and 10 mM of HEPES adjusted to pH 7.4 with NaOH.

For the primary compound screening and the generation of concentration–response curves, a robotic liquid handling station equipped with a 96-tip multichannel head (Freedom Evo 150, Tecan, Männedorf, Switzerland) containing a custom-made fluorescence plate imager was used as described previously (Urban et al., 2016). HEK cells expressing the respective TRP channels were used in trypsinized cell suspensions and loaded with 4 μM of fluo-4-acetoxymethylester (fluo-4/AM) (Invitrogen, Thermo Fisher Scientific, Waltham, MA, USA) in growth medium for 30 min at 37°C. Afterwards, cells were briefly centrifuged and the cell pellets were resuspended in HEPES-buffered solution and dispensed into black pigmented 384-well plates with clear clear-bottom (μClear Greiner, Frickenhausen, Germany). The fluorescence signals were excited with a 470-nm light-emitting diode (LED) array and measured with a cooled Zyla 5.5 camera (Andor, Belfast, UK) through a 515-nm long-pass filter, both synchronized by the camera trigger output. Plates were placed on the imager and μManager software (http://micro-manager.org) was used for image acquisition (Edelstein et al., 2010). After recording a baseline for about 60 s, the compound library or serial dilutions of modulators were applied as duplicates to the cells by the liquid handling station. For the evaluation of inhibitory properties, respective activators were added in a second step. Fluorescence signals were calculated for each well with ImageJ (National Institutes of Health, Bethesda, MD, USA) (Schneider et al., 2012), corrected for background intensities and normalized to the initial signals (ΔF/F$_0$). To generate concentration–response curves, the results were fitted to a four-parameter Hill equation (E$_{min}$, E$_{max}$, Hill coefficient n and EC$_{50}$/IC$_{50}$).

For microfluorometric single-cell [Ca^{2+}]$_i$ imaging, cells were seeded onto 25 mm of coverslips and loaded with 4 μM of fura-2-acetoxymethylester (fura-2/AM) (AAT Bioquest, Sunnyvale, CA, USA) in HEPES-buffered solution containing 0.2% bovine serum albumin (BSA) for 30 min at 37°C. After gentle rinsing with HEPES-buffered solution, coverslips were mounted in a bath chamber. The measurements were performed on an inverted Axiovert 100 microscope (Fluar 10×/0.5, Carl Zeiss, Jena, Germany). The fluorescence signals were excited using a fibre-coupled monochromator device (Polychrome V, TILL Photonics, Gräfelfing, Germany) at alternating wavelengths of 340, 358 and 380 nm and measured with a charge-coupled device (CCD) camera (Sensicam, PCO, Kelheim, Germany) through a dichroic beam splitter DCXR-510 (Chroma, Rockingham, VT, USA) and a 515-nm long-pass filter. Calibration of the [Ca^{2+}]$_i$ was performed as described previously (Lenz et al., 2002). Single-cell traces of representative single-cell recordings are displayed as grey lines and mean response in black.

For LED-total internal reflection fluorescence microscopy, cells were plated onto coverslips and loaded with 10 μM of Cal-520FF-

acetoxymethylester (Cal-520FF/AM) (AAT Bioquest) in HEPES-buffered solution containing 0.2% BSA for 30 min at 37°C. Coverslips were gently washed with HEPES-buffered solution and mounted in a bath chamber. Measurements were performed using an inverted microscope (Zeiss Observer Z1, Carl Zeiss), equipped with an alpha Plan-Apochromat 63×1.46 NA objective (Carl Zeiss) as described previously (Kogel et al., 2019). Fluorescence signals were excited using a high-power LED with a central wavelength of 450 nm (Osram Ostar Stage, Regensburg, Germany), driven with 3 A of constant current and measured with a cooled Orca Quest camera (Hamamatsu, Japan) controlled by the µManager software for image acquisition. Afterwards, a variance analysis over time was performed and visualized with ImageJ (National Institutes of Health). Individual Ca^{2+} sparklets were detected and analysed using the xySpark, Fiji plugin (Steele & Steele, 2014). The spark threshold coefficient was set to 3.6, the Gaussian fit filter threshold to 0.6 and the spatial filter threshold to 5.

2.3 | Electrophysiological procedures

Patch clamp recordings of TRPV2 currents were performed on HEK_{TRPV2} cells in the whole-cell and inside-out configuration using a MultiClamp 700B amplifier with a Digidata 1440A digitizer controlled by the pClamp 10.5 software (all Molecular Devices, Sunnyvale, CA, USA). For whole-cell recordings, the composition of standard extracellular solution was 140 mM of NaCl, 5 mM of CsCl, 2 mM of $MgCl_2$, 1 mM of $CaCl_2$ and 10 mM of HEPES adjusted to pH 7.4 with NaOH and the standard intracellular solution contained 120 mM of Cs-Aspartate, 10 mM of CsCl, 1 mM of $MgCl_2$, 5 mM of ethylene glycol-bis(β-aminoethyl ether)-tetraacetic acid (EGTA) and 10 mM of HEPES adjusted to pH 7.4 with CsOH. For inside-out measurements, symmetrical recording solutions contained 140 mM of NaCl, 2 mM of $MgCl_2$, 0.5 mM of EGTA, 10 mM of glucose and 10 mM of HEPES adjusted to pH 7.2 with NaOH. Patch pipettes were pulled from borosilicate glass capillaries and had a resistance of 3–10 MΩ when filled with intracellular solution. Voltage ramps from -100 to $+100$ mV (500 ms of duration) were applied at 1 s of intervals. Compounds and solutions were applied by using a continuous gravity flow perfusion system. In all whole-cell recordings, the series resistance was <15 MΩ and compensated by 75%. Current densities were calculated to correct for different cell sizes.

2.4 | siRNA-mediated knockdown and reverse transcription quantitative polymerase chain reaction (RT-qPCR)

Stealth siRNA directed against mouse TRPV2 ($siRNA_{mTRPV2}$) (ID: MSS212426) and stealth siRNA negative control ($siRNA_{non-target}$) (med GC) were obtained from Thermo Fisher Scientific (Germany). BMDM were seeded in 96-well plates, T25 flasks or plated onto 25-mm glass coverslips and transfected at a confluency of 60%–90%. A total of 5 pmol (96-well), 50 pmol (coverslip) or 150 pmol (T25 flask) of siRNA

and 0.25 µl (96-well), 5.0 µl (coverslip) or 15 µl (T25 flask) of Lipofectamine™ 2000 (Thermo Fisher Scientific, Germany) were mixed in 50 µl (96-well), 500 µl (coverslip) or 1500 µl (T25 flask) of Opti-MEM I (Gibco Thermo Fisher Scientific). The mixture was incubated for 20 min at room temperature. Afterwards, it was transferred to the cells containing 100 µl (96-well), 1.5 ml (coverslip) or 4.5 ml (T25 flask) of antibiotic-free medium, which was replaced by fresh growth medium after 6–8 h. Experiments were performed after 24–48 h.

RNA was extracted from adherent BMDM or peritoneal macrophages using peqGold TriFast (VWR, Darmstadt, Germany) and 0.1–1 µg of total RNA was subjected to reverse transcription using RevertAid H Minus First Strand cDNA Synthesis Kit (Thermo Fisher Scientific, Waltham, MA, USA), primed with random hexamers. Quantitative PCR was conducted with DyNAmo Flash SYBR Green qPCR Kit (Thermo Fisher Scientific, Waltham, MA, USA) using a PikoReal 24 thermocycler (Thermo Fisher Scientific, Waltham, MA, USA). The following forward and reverse mouse TRPV2 primers were used as published by Sawatani et al. (2019): 5′-TGAT-GAAGGCTGTGCTGAAC-3′ and 5′-CACCACAGGCTCCTCTTCTC-3′. 18S-RNA was used as reference: 5′-TAGAGGGACAAGTGGCGTTC-3′ and 5′-TGTACAAAGGGCAGGGACTT-3′. Primer sets were obtained from Sigma Aldrich. RT-qPCR data were analysed with Ct method.

2.5 | Detection of cell viability

To determine a potential cytotoxicity of compounds, 3-(4,5-dimethylthiazol-2-yl)-2,5-diphenyltetrazolium bromide (MTT) assays were performed. Cells were seeded in 96-well plates at a density of 25,000 cells per well. After 24–48 h, compounds or solvent control were added and cells were incubated for another 24 h before adding 0.5 mg·ml^{-1} of 3-(4,5-dimethylthiazol-2-yl)-2,5-diphenyltetrazolium bromide with new medium for 3 h. Afterwards, supernatants were aspirated and the absorbance of formazan dissolved in DMSO was measured at 560 and 670 nm with a plate reader (POLARstar Omega, BMG Labtech, Germany). To analyse the data, the differences of both extinctions were calculated and the results were normalized to solvent control.

2.6 | Phagocytosis and LPS-induced migration assays

For phagocytosis assays, BMDM were seeded into 96-well plates at a density of 30,000–50,000 cells per well. After adhesion, equilibration and, depending on the experiment, siRNA-mediated knockdown, BMDM were polarized for 24 h as described above. Medium was replaced by HEPES-buffered solution and the cells were allowed to equilibrate for 30 min at 37°C. Respective compounds or solvent control and pHrodo-labelled zymosan or *S. aureus* bioparticles were added and incubated for another 1 h at 37°C. The fluorescence of phagocytosed bioparticles was excited using a 505/10-nm band-pass filter and measured through a 540/10-nm band-pass filter with a plate reader

(POLARstar Omega, BMG Labtech). Data were analysed as phagocytosis activity normalized to bioparticles-treated control BMDM.

The migration assay was performed in 24-well plates with transwell inserts (translucent, 8-μm pore size, Greiner, Frickenhausen, Germany) using culture medium with a reduced FCS concentration of 1% (migration medium) to monitor chemoattractant-mediated migration. After transfection with siRNA, depending on the experiment and polarization, BMDM were starved in migration medium for 1–2 h, harvested and seeded into the upper chamber of 24-well inserts at a density of 40,000–50,000 cells together with respective compounds or corresponding solvent control. The lower chamber contained migration medium supplemented with 100 ng·ml^{-1} of LPS and respective compounds or solvent control. After 14 h at 37°C in a 5% CO_2-aerated, humidified atmosphere, the inserts were gently washed three times with HEPES-buffered solution, fixed with −20°C cold methanol and stained with a 0.2% crystal violet dye solution. Cells in the upper compartment were gently removed and cells on the lower side of the filter were counted in three random visual fields using an inverted Axiovert 100 microscope (LD Achroplan 40×/0.6, Carl Zeiss). Data were analysed as migrated cells normalized to an untreated control.

2.7 | Data and statistical analysis

Data and statistical tests in this study comply with the recommendations of the *British Journal of Pharmacology* on experimental design and analysis in pharmacology (Curtis et al., 2022). Studies were designed to randomly generate groups of equal size. Blinding was not performed for this study as all experiments revealed strict quantitative data. Cell culture dishes were randomly assigned to various treatments. Studies were designed to generate groups of equal sizes. The results are presented as means and standard deviation (SD) of at least 5 per group (stated as n in the figure legend) or as means and standard error of the mean (SEM) of 5 independent experiments. The declared group size is the number of independent values and statistical analysis was done using these independent values. Normalization of individual datasets was performed for determination of EC_{50} to reduce variability in baseline between independent experiments and for analysis of Ca^{2+} sparklets as the number of imaged cells varied in each experiment. Datasets were compared using one-way analysis of variance (ANOVA) followed by a Bonferroni post hoc test after variance homogeneity was confirmed by Levene's test and normality distribution by Shapiro–Wilk's test. RT-qPCR data were log-transformed before statistical analysis. For statistical evaluation of TRPV2-mediated Ca^{2+} sparklets, data were compared using ANOVA with repeated measurements, followed by a Bonferroni post hoc test. Normality of distribution of non-normalized data was confirmed by Shapiro–Wilk's test and variance homogeneity was confirmed by Brown–Forsythe's tests. Post hoc tests were conducted only if F in ANOVA achieved $P < 0.05$. $P < 0.05$ was considered as being statistically significant (*$P < 0.05$). The half-maximal inhibitory effect (IC_{50}) was determined by fitting the data to Hill's equation. All statistical analysis was performed using OriginPro 2019 (OriginLab Corporation, Northampton, MA, USA).

2.8 | Materials

The compound library was obtained from the Molecule Archive at the Karlsruhe Institute of Technology (Jung et al., 2016). The synthesis and purification of the inhibitors 5-(1,3-dithiolan-2-ylidene)-4-methyl-5-phenylpentan-2-one (IV2-1), 4-[1,3-dithiolan-2-ylidene(phenyl)methyl]-5-methylhexan-2-one (IV2-2) and 5-(1,3-dithiolan-2-ylidene)-4-methyl-5-phenyl-pentan-2-ol (IV2-3) are described fully in supplementary data under the section - Compound Synthesis. The structure of these compounds is also shown in Figure 1b. Contact: compound-platform@ioc.kit.edu for requests. These compounds were dissolved in dimethyl sulfoxide (DMSO) to a stock concentration of 100 mM. Valdecoxib (100 mM of stock in DMSO), 2-APB (1 M of stock in DMSO), capsaicin (10 mM of stock in DMSO), GSK1016790A (10 mM of stock in DMSO), lipopolysaccharide (LPS) from *Escherichia coli* O111:B4 (1 mg·ml^{-1} of stock in water) and cytochalasin D (2 mM in DMSO) were purchased from Sigma Aldrich (Munich, Germany). Probenecid (400 mM of stock in 0.5 M of NaOH solution) was obtained from Hycultec (Beutelsbach, Germany). DMSO concentrations on cells did not exceed 0.1%. Both pHrodo Green Zymosan Bioparticles Conjugate for Phagocytosis and pHrodo Green *Staphylococcus aureus* Bioparticles Conjugate for Phagocytosis were obtained from Thermo Fisher Scientific (P35367 and P35365, Darmstadt, Germany). Recombinant murine macrophage colony-stimulating factor (M-CSF) was purchased from PeproTech (Hamburg, Germany). Foetal calf serum was purchased from Thermo Fisher Scientific geneticin was obtained from Capricorn Scientific (Ebsdorfegrund, Germany). Cell culture medium and supplements as well as all other chemicals, if not stated otherwise, were purchased from Sigma Aldrich. Details of other materials and suppliers are provided in the specific sections.

2.9 | Nomenclature of targets and ligands

Key protein targets and ligands in this article are hyperlinked to corresponding entries in the IUPHAR/BPS Guide to PHARMACOLOGY http://GRAC and are permanently archived in the Concise Guide to PHARMACOLOGY 2021/22 (Alexander et al., 2021).

3 | RESULTS

3.1 | Heterologously expressed TRPV2 channels are blocked by IV2-1

As the pharmacology of TRPV2 channels is still scant, we aimed at identifying novel compounds targeting TRPV2 channels. In this context, we recently demonstrated that valdecoxib, a COX-2 inhibitor, is also a novel rat TRPV2 inhibitor (Bluhm et al., 2022). However, despite a selectivity for TRPV2 within the TRPV subfamily, COX-2 inhibitors induce different effects on various other ion channels (Frolov & Singh, 2014; Spyra et al., 2017). Therefore, we conducted a medium-throughput screening using a compound library of 4000
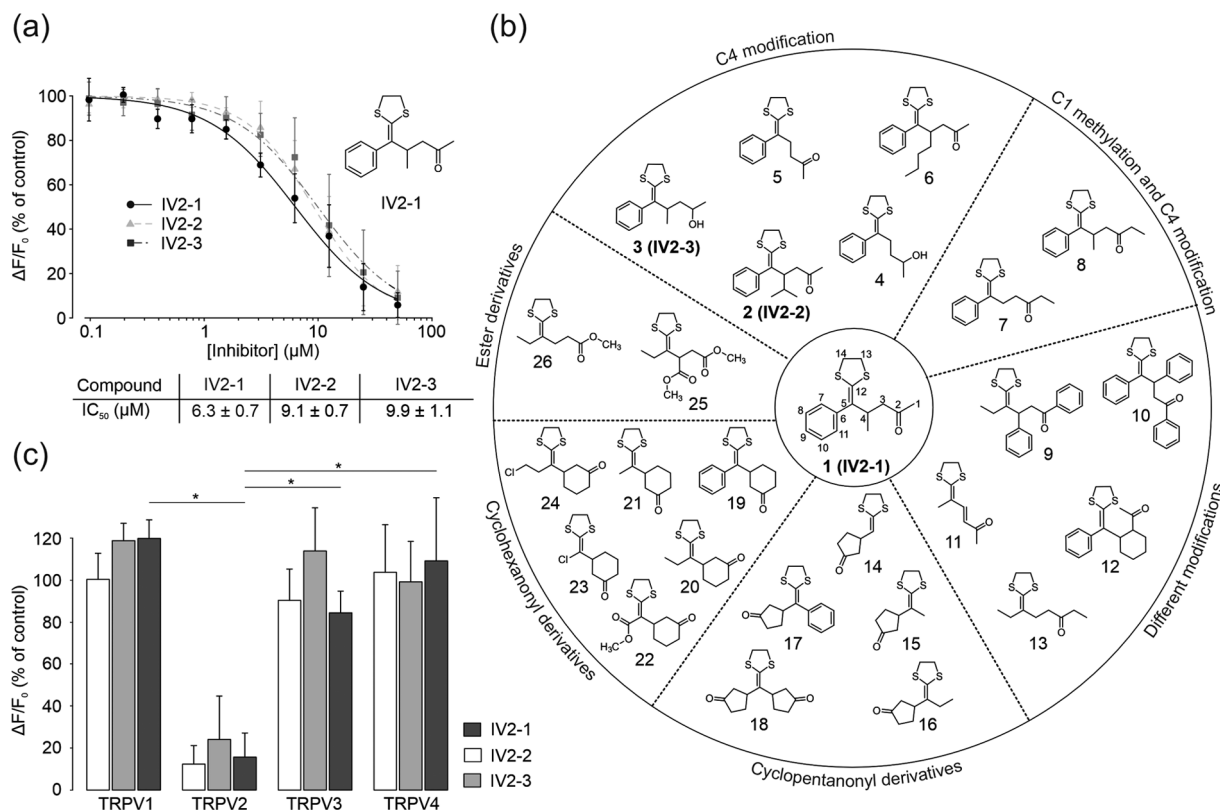
FIGURE 1 (a) Inhibitory concentration–response analysis of inhibitor 5-(1,3-dithiolan-2-ylidene)-4-methyl-5-phenylpentan-2-one (IV2-1) (IC_{50} = 6.3 ± 0.7 μM), IV2-2 (IC_{50} = 9.1 ± 0.7 μM) and IV2-3 (IC_{50} = 9.9 ± 1.1 μM) in fluo-4-acetoxymethylester-loaded HEK_{TRPV2} cell suspensions activated with 300 μM of 2-aminoethoxydiphenyl borate (2-APB). Shown are means ± SD of n = 5 independent experiments (carried out as duplicates). (b) Chemical structures of IV2-1, 4-[1,3-dithiolan-2-ylidene(phenyl)methyl]-5-methylhexan-2-one (IV2-2), 5-(1,3-dithiolan-2-ylidene)-4-methyl-5-phenyl-pentan-2-ol (IV2-3) and chemically related compounds. (c) Selectivity analysis of IV2-1, IV2-2 and IV2-3 (25 μM) in human embryonic kidney 293 (HEK293) cells stably expressing the respective channel, activated with 2 μM of capsaicin (transient receptor potential vanilloid 1 [TRPV1]), 300 μM of 2-APB (TRPV2), 100 μM of 2-APB (TRPV3) or 1 μM of GSK1016790A (TRPV4). Depicted are means ± SD of n = 5 independent experiments.

chemically diverse molecules (Molecule Archive, ComPlat) to identify novel and more selective TRPV2-modulating compounds (Jung et al., 2016). The individual compounds were added at concentrations of 20 μM to fluo-4-acetoxymethylester-loaded HEK_{TRPV2} cells to identify activators, followed by 300 μM of 2-APB to identify possible TRPV2-blocking compounds. After initial validation of primary hits, we performed a secondary screen focussing on 1500 additional compounds with chemical similarity to the hits of the primary screen and identified the three dithiolanes IV2-1, IV2-2 and IV2-3 (Figure 1b; see supplementary data -compound synthesis section) as novel TRPV2 blockers (the dot blot high-throughput screening (HTS) graph of the initial screen is shown in Figure S1). Fluorometric concentration–response analysis of the three hits revealed IC_{50} values from 6.3 to 9.9 μM for the inhibition of 2-APB-activated rTRPV2 channels, indicating moderate potencies (Figure 1a). In contrast, 66 chemically related compounds showed no activity at a concentration of 20 μM (Figure 1b), providing initial information of a structure–activity relationship. Although C4 modifications, such as an isopropyl group were tolerated (Figure 1b, 1–3), bulky groups, for example a butyl group or a removal of the methyl group, resulted in a loss of activity (Figure 1b,

4–6). In addition, a small C1 methylation caused a loss of activity (Figure 1b, 7 and 8). Restricting the steric flexibility of the hydroxyl or ketone group (Figure 1b, 15) also resulted in an inactive compound. We next tested the selectivity of the three blockers IV2-1, IV2-2 and IV2-3 within the TRPV family. The blockers showed no effects at concentrations up to 50 μM on rat TRPV1, mouse **TRPV3** or mouse **TRPV4** channels stably expressed in HEK293 cells after activation with their respective agonists:- **capsaicin** (TRPV1), 2-APB (TRPV3) or **GSK1016790A** (TRPV4) (Figures 1c and S2). As IV2-1 blocked TRPV2 with the highest potency, it was utilized for further studies.

The ability of IV2-1 to block TRPV2-mediated increases in $[Ca^{2+}]_i$ was confirmed in calibrated microfluorometric single-cell analysis in fura-2-acetoxymethylester-loaded HEK_{TRPV2} cells (Figure 2a,b) using 2-APB to activate TRPV2 channels (Figure 2a). We have previously described that co-application of different TRPV2 activators exerts super additive effects on TRPV2 (Bluhm et al., 2022). Accordingly, the application of a low 2-APB concentration (30 μM), which did not activate TRPV2 channels on its own, induced robust TRPV2-mediated increases in $[Ca^{2+}]_i$ when combined with 500 μM of probenecid (Figure 2b). Responses were completely blocked after addition of
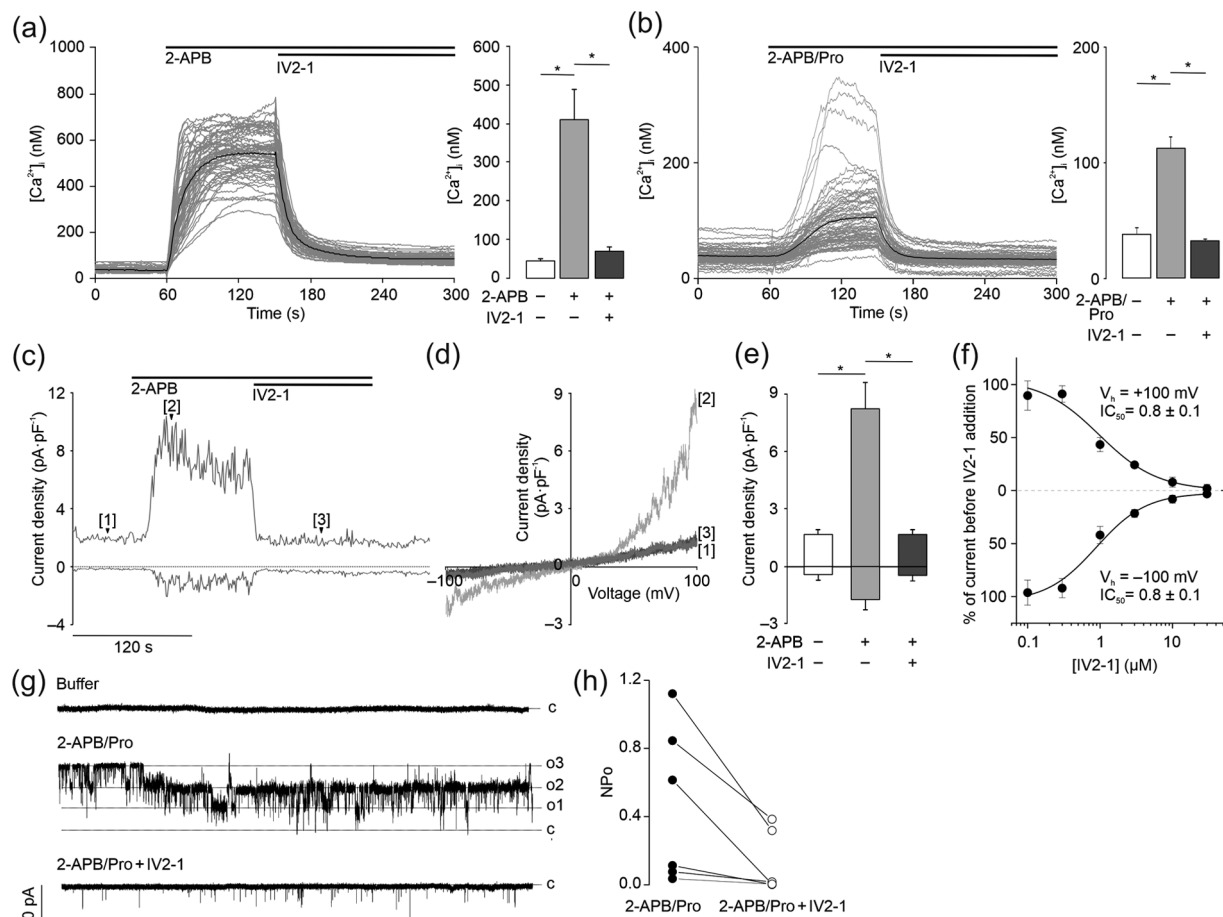
FIGURE 2 Microfluorometric single-cell analysis of $[Ca^{2+}]_i$ in fura-2-acetoxymethylester-loaded HEK$_{TRPV2}$ cells, activated with 300 μM of 2-aminoethoxydiphenyl borate (2-APB) (a) or 30 μM of 2-APB/500 μM of probenecid (Pro) (b) before and after addition of 20 μM of inhibitor 5-(1,3-dithiolan-2-ylidene)-4-methyl-5-phenylpentan-2-one (IV2-1). Depicted are example time courses and statistical analysis with means ± SD of n = 5 independent experiments. (c) Time course of whole-cell current densities averaged at Vm = +100 and −100 mV in HEK$_{TRPV2}$ cells in response to application of 300 μM of 2-APB and 20 μM of IV2-1 extracted from voltage ramps as in (d). (e) Statistical analysis depicting means ± SD of n = 6 independent experiments such as in (c). (f) Inhibitory concentration–response analysis of IV2-1 blocking 400 μM of 2-APB-elicited inward (IC_{50} = 0.8 ± 0.1 μM) and outward (IC_{50} = 0.8 ± 0.1 μM) currents depicted as means ± SD of n = 5 independent experiments. (g) Example recording of an inside-out patch, pulled from a HEK$_{TRPV2}$ cell at V_h = −70 mV, before (buffer), after addition of the 2-APB (100 μM)/Pro (1 mM) combination and after addition of IV2-1 (20 μM). c refers to the closed state of the channels and o1–o3 refer to the openings of individual channels. (h) Statistical analysis of 6 independent experiments such as in (g) depicting open probabilities (NPo) obtained from 30 s of intervals after activation (filled circles) and after addition of IV2-1 (open circles).

IV2-1. No increases in $[Ca^{2+}]_i$ occurred in the parental HEK cell line (Figure S3a). In a next step, we performed electrophysiological patch clamp experiments on HEK$_{TRPV2}$ cells. 2-APB elicited typical inwardly rectifying TRPV2 currents with a reversal potential close to 0 mV, which were inhibited upon addition of 20 μM of IV2-1 (Figure 2c–e). Electrophysiological concentration–response analysis revealed an IC_{50} of 0.8 ± 0.1 μM for the block of the inward and outward currents (Figure 2f) In inside-out patches, a 2-APB/probenecid combination elicited single-channel openings (Figure 2g). Again, the addition of 20 μM of IV2-1 strongly reduced the open probability of TRPV2 channels (Figure 2g,h), demonstrating the ability of IV2-1 to block TRPV2 in a membrane-delimited manner. Proliferation assays utilizing HEK293 or HEK$_{TRPV2}$ cells demonstrated no acute cellular toxicity or a reduction of metabolic activity after addition of IV2-1 at

concentrations up to 50 μM for 24 h (Figure S3b). Taken together, these results emphasized the applicability of IV2-1 for further cellular assays.

3.2 | Inhibiting TRPV2 in primary rat macrophages

As a high expression of TRPV2 has been demonstrated in macrophages (Nagasawa et al., 2007; Yamashiro et al., 2010), monocytes from mouse bone marrow were isolated and differentiated into macrophages (Yamashiro et al., 2010). Single-cell calcium assays revealed 2-APB-elicited increases in $[Ca^{2+}]_i$, which were strongly reduced, when cells were pre-treated with 20 μM of IV2-1, confirming the functional expression of TRPV2 in mouse macrophages and the
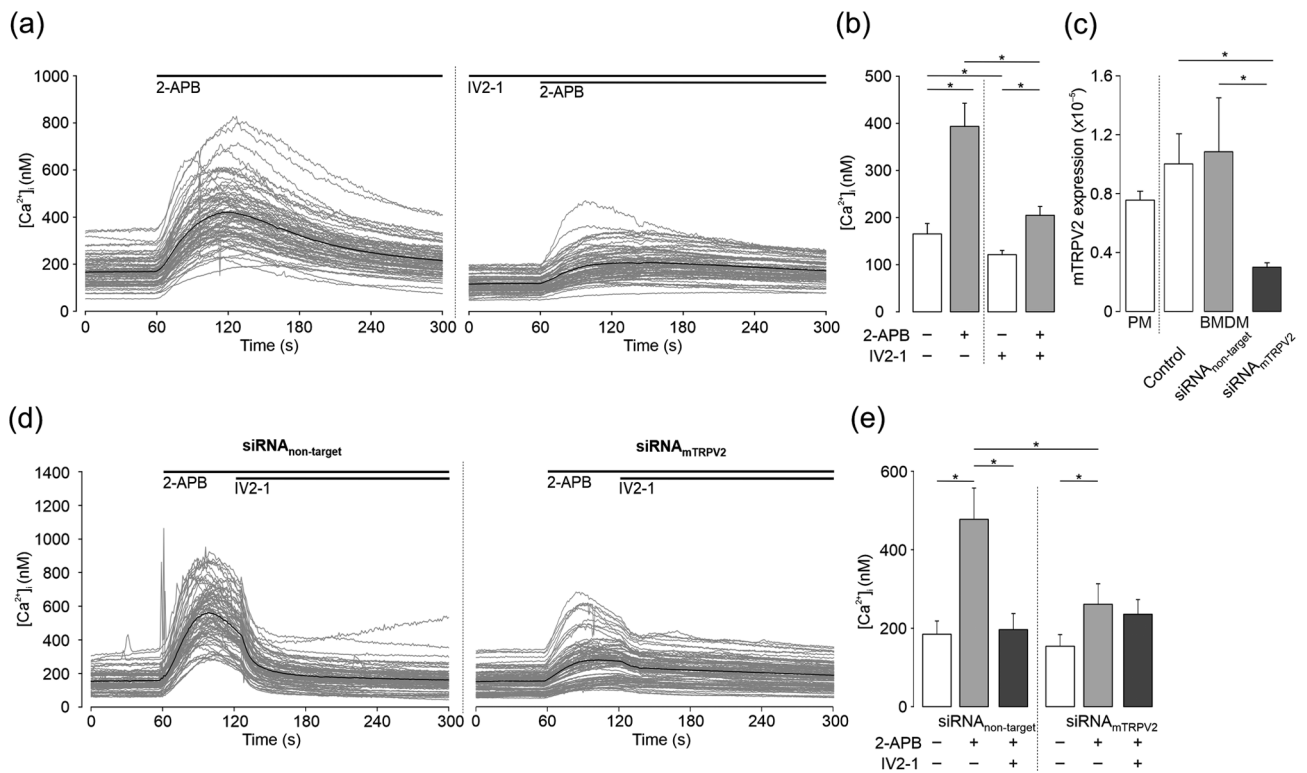
FIGURE 3   (a) Microfluorometric single-cell analysis of $[Ca^{2+}]_i$ in fura-2-acetoxymethylester (fura-2/AM)-loaded bone marrow-derived macrophages (BMDM) activated with 300 μM of 2-aminoethoxydiphenyl borate (2-APB) with or without pre-incubation with 20 μM of inhibitor 5-(1,3-dithiolan-2-ylidene)-4-methyl-5-phenylpentan-2-one (IV2-1). (b) Statistical analysis depicting means ± SD of n = 5 independent experiments as in (A). (c) Reverse transcription quantitative polymerase chain reaction analysis of transient receptor potential vanilloid 2 (TRPV2) mRNA expression in primary peritoneal macrophages (PM), BMDM and BMDM after transfection of $siRNA_{mTRPV2}$ or $siRNA_{non-target}$, shown as means ± SD of n = 5 independent experiments. (d) Microfluorometric single-cell analysis of $[Ca^{2+}]_i$ in fura-2/AM-loaded BMDM transfected with $siRNA_{non-target}$ or $siRNA_{mTRPV2}$ before and after addition of 300 μM of 2-APB and 20 μM of IV2-1 as example time courses. (e) Statistical analysis depicting means ± SD of n = 5 independent experiments as in (d).

applicability of IV2-1 in such cells (Figure 3a,b). Accordingly, siRNA-mediated knockdown of TRPV2 decreased the expression of TRPV2 in BMDM by about 70% (Figure 3c) and resulted in significantly lower 2-APB-elicited increases in $[Ca^{2+}]_i$ than BMDM treated with control siRNA (Figure 3d,e).

We next wanted to investigate how acute block of TRPV2 channels in BMDM by IV2-1 or valdecoxib affects phagocytic activity and migration of BMDM. To this end, macrophage-mediated phagocytosis assays were performed using pHrodo-labelled zymosan or *S. aureus* bioparticles. The inhibition of TRPV2 by IV2-1, valdecoxib or siRNA-mediated knockdown attenuated phagocytosis of zymosan or *S. aureus* bioparticles to about 70% of control cells treated with non-target siRNA (Figure 4a,b), emphasizing a contribution of TRPV2 in phagocytosis. Incubation of BMDM with IV2-1 or valdecoxib for 24 h showed no reduction of metabolic activity at concentrations up to 50 μM (Figure 4c), confirming the applicability of the two structurally different TRPV2 blockers in BMDM.

To further investigate the role of TRPV2 in chemoattractant-induced migration of macrophages, we applied the combination of 30 μM of 2-APB and 500 μM of probenecid to activate TRPV2. In contrast to 300 μM of 2-APB, this combination showed no cytotoxic

effects even when simultaneously applied with IV2-1 or valdecoxib for 24 h (Figure 4c,d). Next, we performed a two-dimensional trans-well migration assay with BMDM in an LPS gradient (Figure 4f,g). While control $siRNA_{non-target}$ showed no effects, the siRNA-mediated knockdown of TRPV2 led to an attenuated migration of BMDM. Moreover, TRPV2 inhibition by IV2-1 or valdecoxib also attenuated migration of BMDM, confirming the involvement of TRPV2 in macrophage migration. In contrast, activating TRPV2 with the 2-APB/probenecid combination significantly enhanced the number of migrated cells. This effect was inhibited by IV2-1, valdecoxib or siRNA-mediated knockdown of TRPV2.

3.3 | TRPV2 generates Ca^{2+} microdomains in macrophages

For cellular migration, Ca^{2+}-dependent signalling cascades play a crucial role as they may induce, for example, directional sensing, cytoskeletal rearrangement or actin polymerization (Wei et al., 2009). As we could show that TRPV2-mediated Ca^{2+} influx contributes to macrophage-mediated phagocytosis and migration, we investigated
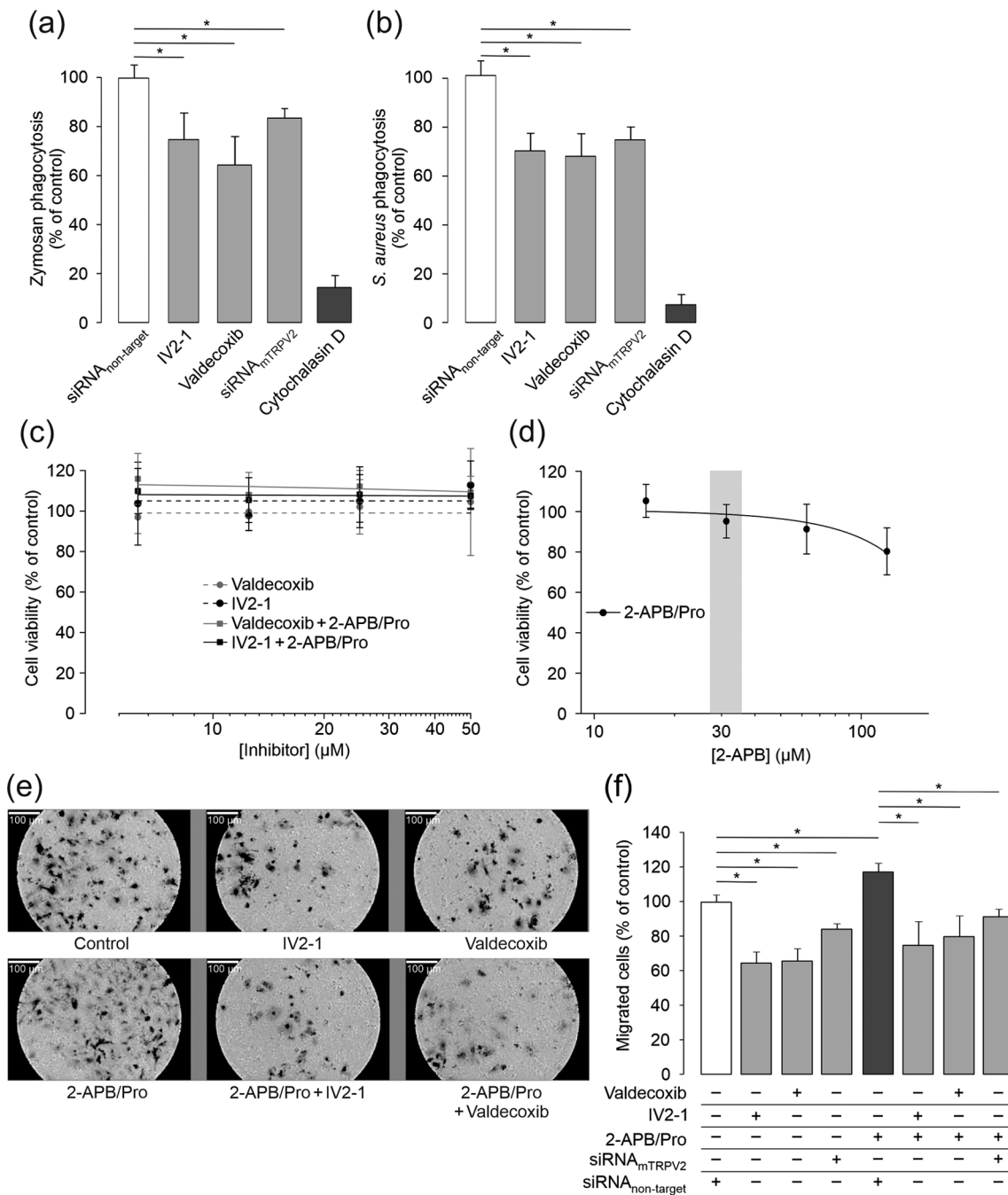
FIGURE 4 (a, b) Phagocytosis assays using pHrodo-labelled zymosan (a) or *Staphylococcus aureus* (b) bioparticles and bone marrow-derived macrophages (BMDM) treated with 20 μM of inhibitor 5-(1,3-dithiolan-2-ylidene)-4-methyl-5-phenylpentan-2-one (IV2-1), 20 μM of valdecoxib, 2 μM of cytochalasin D, siRNA$_{non\text{-}target}$ or siRNA$_{mTRPV2}$. Data show fluorescence signals of phagocytized bioparticles in percentage of non-treated control group as means ± SD of n = 5 independent experiments. (c, d) Concentration–response analysis of IV2-1 and valdecoxib, the presence or absence of 30 μM of 2-aminoethoxydiphenyl borate (2-APB)/500 μM of probenecid (Pro) (c) or 2-APB combined with 500 μM of Pro (d) measured as cell viability with BMDM after 24 h using 3-(4,5-dimethylthiazol-2-yl)-2,5-diphenyltetrazolium bromide (MTT) assays depicted as means ± SD of n = 5 independent experiments. (e, f) Trans-well migration assay using BMDM, treated with 20 μM of IV2-1, 20 μM of valdecoxib, 30 μM of 2-APB/500 μM of Pro, siRNA$_{mTRPV2}$ or siRNA$_{non\text{-}target}$ and a lipopolysaccharide gradient for 14 h. Depicted are representative examples of crystal violet dyed inserts (f) and statistical analysis of migrated cells as percentage of a non-treated control group as means ± SD of n = 6 independent experiments (g).

whether TRPV2 activation may cause spatially and temporally confined Ca^{2+} microdomains. Using total internal reflection fluorescence microscopy in combination with the low affinity Ca^{2+} indicator Cal-

520FF-acetoxymethylester, we were able to monitor local increases in [Ca^{2+}]$_i$ in the immediate proximity to the plasma membrane after addition of 30 μM of 2-APB/500 μM of probenecid. These
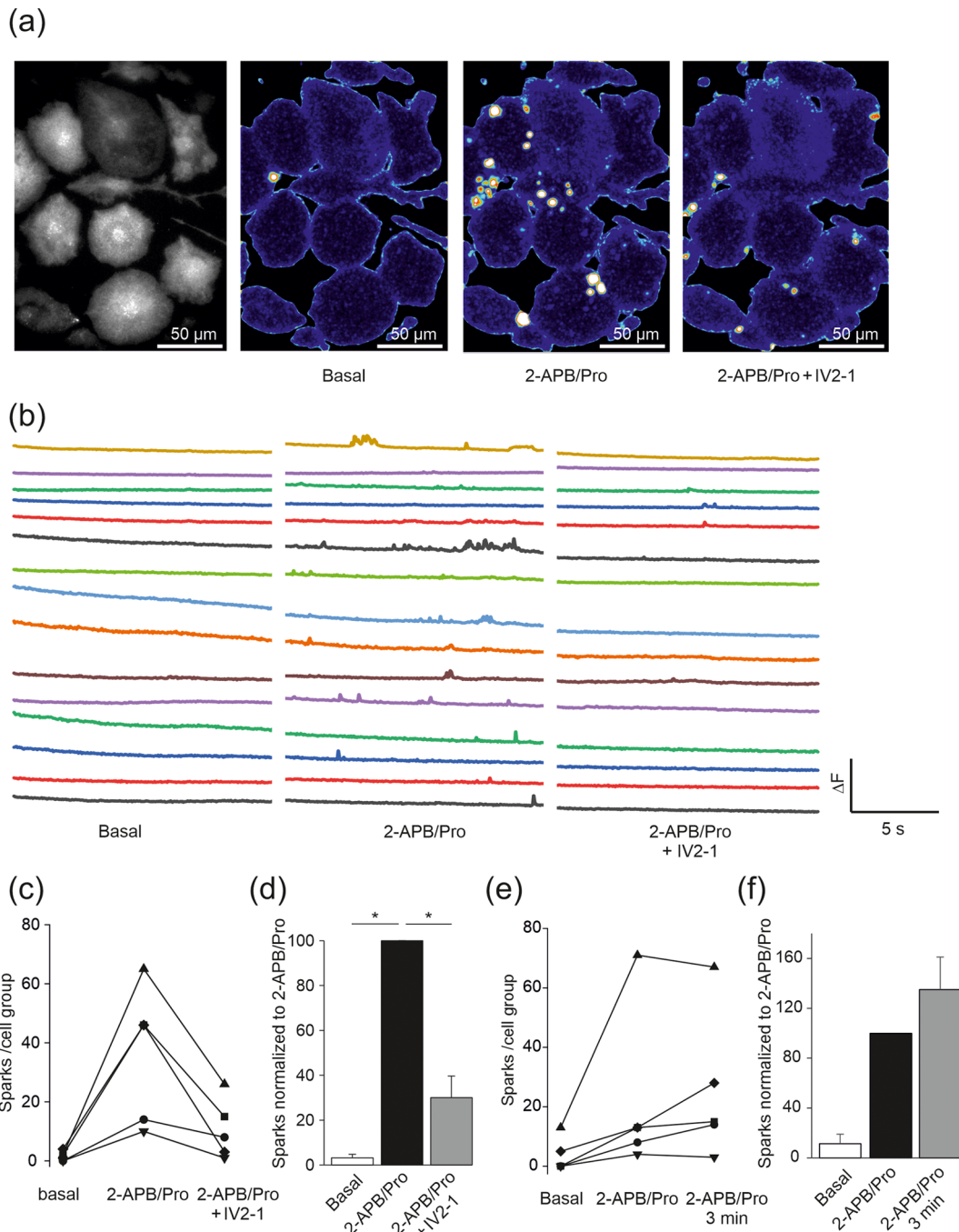
FIGURE 5 (a, b) Microfluorometric single-cell analysis of Ca^{2+} sparklets in Cal-520FF-acetoxymethylester-loaded bone marrow-derived macrophages at room temperature before and after application of 30 μM of 2-aminoethoxydiphenyl borate (2-APB)/500 μM of probenecid (Pro) and 20 μM of inhibitor 5-(1,3-dithiolan-2-ylidene)-4-methyl-5-phenylpentan-2-one (IV2-1), monitored by total internal reflection fluorescence microscopy. (a) Imaged cell groups depicted as an example picture (left panel) or variance analysis (other panels). Shown are maximum projection of variation coefficients calculated over bins of five consecutive images before (basal) or after addition of 2-APB/Pro and IV2-1. Pseudocolour scale ranges from 0 to 10. (b) Example time courses of Ca^{2+} fluctuations (in arbitrary units [a.u.]) in representative microdomains/Ca^{2+} sparklets over a time period of 15 s. (c) Number of sparklets in individual imaged cell groups before and after addition of 2-APB/Pro and IV2-1. For each condition, sparklets were registered for a 15-s time period. Data are presented as scatter plots of paired measurements under three conditions (basal, after addition of 2-APB/Pro and after addition of IV2-1). (d) Statistical analysis of Ca^{2+} events under the three conditions. Data were normalized to number of Ca^{2+} events after addition of 2-APB/Pro and are depicted as means ± SEM of n = 5 independent experiments. (e) Same experiment as in (a)–(d) but without addition of IV2-1. (f) Statistical analysis of Ca^{2+} sparklets as in (d). Data are depicted as means ± SEM of n = 5 independent experiments.

TRPV2-mediated Ca^{2+} sparklets were presumably generated by single or few channels predominantly located at the margins of the BMDM and were significantly reduced after treatment of the cells with IV2-1 (Figure 5a–d), whereas no reduction in the number of Ca^{2+} sparklets was obvious over the same time period in the absence of the TRPV2 inhibitor IV2-1 (Figure 5e,f). This clearly indicates that TRPV2 activity is critically involved in the formation of Ca^{2+} microdomains.

4 | DISCUSSION

Despite large progress in the TRP channel field, the role of TRPV2 in physiological and pathophysiological states remains largely unknown. Due to the absence of selective activators of TRPV2, commonly used compounds are non-selective such as 2-APB, probenecid or cannabinoids such as cannabidiol or Δ^9-tetrahydrocannabinol (Bang et al., 2007; Colton & Zhu, 2007; Qin et al., 2008). To activate TRPV2, high concentrations of these compounds are required, which additionally exert a multitude of unselective and cytotoxic effects. Besides a modulation of cannabinoid CB_1 or CB_2 receptors, Δ^9-tetrahydrocannabinol also activates TRP ankyrin 1 (TRPA1) and induces TRPV1 activity (Jordt et al., 2004; Qin et al., 2008). While probenecid inhibits organic anion transporters, cystic fibrosis transmembrane conductance regulators or swelling-activated anion channels (Darby et al., 2003; Diena et al., 2007), 2-APB inhibits store-operated channels, inositol-1,4,5-triphosphate receptors or sarcoendoplasmic reticulum calcium ATPase (SERCA) pumps (Bootman et al., 2002). In addition, 2-APB blocks the release of Ca^{2+} sequestered in mitochondria and induces the non-specific leak of Ca^{2+} from intracellular Ca^{2+} stores (Bootman et al., 2002; Missiaen et al., 2001). Regarding TRP channels, 2-APB activates TRPV1 and TRPV3 and blocks several channels of the TRP canonical (TRPC) subfamily and TRP melastatin 2 (TRPM2) (Colton & Zhu, 2007; Nazıroğlu et al., 2011). Therefore, functional assays, which require a longer incubation with TRPV2-activating compounds, are often hampered by cytotoxicity and off-target cellular effects of these drugs. The approach of combining 2-APB and probenecid has recently been demonstrated to exert super additive effects on TRPV2 channels (Bluhm et al., 2022), enabling us to reduce activator concentrations by a factor of 10. The simultaneous application of 2-APB together with probenecid induced a robust activation of TRPV2 without detectable cytotoxic effects in HEK_{TRPV2} cells and primary macrophages. Frequently used TRPV2 inhibitors, such as ruthenium red, tranilast or SKF96365 are non-selective for TRPV2 and exhibit cytotoxic effects as well. We have recently introduced the COX-2 inhibitor valdecoxib as a novel inhibitor of rat TRPV2 channels. Here, we further complement the range of available TRPV2 inhibitors by introducing the structurally different dithiolane IV2-1 as a novel TRPV2-selective inhibitor. The non-toxic IV2-1 blocks TRPV2 with a moderate potency and the discrepancy between the fluorometric (6.3 ± 0.7 μM) and electrophysiological (0.8 ± 0.1 μM) IC_{50} values may occur due to modified cellular conditions in patch clamp experiments that directly affect TRPV2, such as alterations of the plasma membrane or a strongly buffered $[Ca^{2+}]_i$. With

the novel set of activators and inhibitors, we are now able to acutely modulate TRPV2 in primary macrophages and reduce the probability of off-target effects at the same time.

The expression of TRPV2 in macrophages has already been reported (Entin-Meer & Keren, 2020; Link et al., 2010; Yamashiro et al., 2010) and migration, particle binding and phagocytosis are believed to be dependent on appropriate TRPV2 function (Entin-Meer & Keren, 2020; Koyasu, 2010). As bacterial infection in TRPV2 knockout mice resulted in a reduced bacterial clearance and an accelerated mortality, there is evidence that TRPV2 recruitment to nascent phagosomes followed by Fcγ receptor clustering and depolarization is part of particle binding and macrophage-mediated phagocytosis (Link et al., 2010). In accordance, in cystic fibrosis macrophages, the impaired phagocytic activity might be caused by deregulated TRPV2 signalling (Grebert et al., 2019). However, these results are mainly based on knockdown or knockout models, which bear the risk of genetic compensation mechanisms. The use of pharmacological modulators enables acutely blocking or activating TRPV2 channels in cells derived from different species to confirm the role of TRPV2 as determined in knockout approaches. We here confirm the functional expression of TRPV2 in primary macrophages and its involvement in phagocytic activity of BMDM. Either TRPV2 might be activated downstream of toll-like receptor (TLR) signalling or a basal TRPV2 conductivity, recently suggested by Link et al., might be required for phagocytosis (Lévêque et al., 2018; Link et al., 2010). Consequently, such increase in $[Ca^{2+}]_i$ might further mediate actin polymerization, which facilitates changes in the cytoskeleton necessary for phagocytosis. Modified dynamics of actin polymerization might also affect motility and migration of macrophages (Entin-Meer & Keren, 2020; Koyasu, 2010; Link et al., 2010), and here we show that TRPV2 activation promotes chemoattractant-induced migration of macrophages. Moreover, TRPV2 inhibition leads to an attenuated migration towards an LPS gradient, underlining the physiological relevance of a basal TRPV2 activity for appropriate macrophage function.

In macrophage-mediated phagocytosis, TRPV2 signalling might be strongly dependent on channel localization (Lévêque et al., 2018). When stimulated, macrophages undergo a highly ordered rearrangement of the plasma membrane to prepare for phagocytosis (Magenau et al., 2011). In this context, the organization of TRPV2 in lipid microdomains might induce highly fluctuating and locally restricted Ca^{2+} signals (Brundage et al., 1991; Wei et al., 2009). Additionally, organization of TRPV2 in microdomains that are enriched in steroids such as cholesterol and sphingolipids might directly affect channel activity by increased surface expression or spatial convergence to phosphorylating or regulating structures (Bobkov & Semenova, 2022; Sághy et al., 2015; Svobodova & Groschner, 2016). Therefore, we wanted to investigate whether TRPV2 shapes Ca^{2+} microdomains by performing total internal reflection fluorescence microscopy in combination with a low affinity Ca^{2+} indicator, which enabled the localization of sub-plasmalemmal Ca^{2+} microdomains in BMDM (Lock et al., 2015). Indeed, TRPV2 activity generated sparklets of micromolar Ca^{2+} concentration by single or few channels predominantly located at the

margin of the cells. Hence, we provide evidence that TRPV2 shapes Ca^{2+} microdomains in regions of the cell that are strategically important to support phagocytosis. These locally limited high fluctuations of the Ca^{2+} concentration may further mediate actin polymerization dynamics by myosin light chain kinase as part of a targeted chemoattractant-linked migration (Levin et al., 2016; Wei et al., 2009). A Ca^{2+}-dependent induction of protein kinase C activity is also conceivable, which may reveal a phosphorylation of various targets that support phagocytosis or migration (Levin et al., 2016). Additionally, a TRPV2-mediated elevation of the Ca^{2+} concentration and membrane depolarization may activate co-localized high conductance voltage- and **Ca^{2+}-gated K^+ (BK)** or **proton (H_v1)** channels in microdomains, which for example directly affect respiratory bursts (Morera et al., 2015).

In conclusion, we here present the small-molecule IV2-1 as a novel TRPV2 blocker, which blocks the increase of $[Ca^{2+}]_i$ and ionic currents mediated by rat TRPV2 channels with an IC_{50} of 6.3 or 0.8 μM, respectively. As IV2-1 does not mediate any effects on TRPV1, TRPV3 and TRPV4, it enables the distinction between different TRPV channels, when simultaneously expressed in tissues. IV2-1 does not exert cytotoxic effects on primary macrophages at concentrations up to 50 μM. By combining two different TRPV2 activators, we were able to efficiently and acutely modulate TRPV2 channels in phagocytosis and migration assays. Moreover, we here provide evidence that TRPV2 activation shapes Ca^{2+} microdomains in macrophages, which are responsible for a locally restricted Ca^{2+} influx. Therefore, IV2-1 constitutes a fruitful lead compound for further *in vitro* and *in vivo* studies to investigate physiological signalling of TRPV2 in immunological processes.

DECLARATION OF TRANSPARENCY AND SCIENTIFIC RIGOUR

This Declaration acknowledges that this paper adheres to the principles for transparent reporting and scientific rigour of preclinical research as stated in the *BJP* guidelines for Design and Analysis, Immunoblotting and Immunochemistry and Animal Experimentation, and as recommended by funding agencies, publishers and other organizations engaged with supporting research.

AUTHOR CONTRIBUTIONS

Rick Raudszus: Conceptualization (equal); formal analysis (equal); investigation (equal); writing—original draft (equal). **Andrea Paulig:** Formal analysis (equal); investigation (equal). **Nicole Urban:** Investigation (equal). **Anke Deckers:** Project administration (equal). **Simone Gräßle:** Investigation (equal). **Sylvia Vanderheiden:** Investigation (equal). **Nicole Jung:** Supervision (equal); writing—original draft (equal). **Stefan Bräse:** Funding acquisition (equal); project administration (equal). **Michael Schaefer:** Conceptualization (equal); funding acquisition (equal); project administration (equal); supervision (equal). **Kerstin Hill:** Conceptualization (equal); formal analysis (equal); funding acquisition (equal); investigation (equal); project administration (equal); supervision (equal); writing—original draft (equal); writing—review and editing (equal).

CONFLICT OF INTEREST STATEMENT

The authors declare no conflicts of interest.

DATA AVAILABILITY STATEMENT

The data that support the findings of this study are available from the corresponding author upon reasonable request. Some data may not be made available because of privacy or ethical restrictions.

ORCID

Michael Schaefer https://orcid.org/0000-0003-3662-4387
Kerstin Hill https://orcid.org/0000-0003-1306-8824

REFERENCES

Alexander, S. P., Mathie, A., Peters, J. A., Veale, E. L., Striessnig, J., Kelly, E., Armstrong, J. F., Faccenda, E., Harding, S. D., Pawson, A. J., Southan, C., Davies, J. A., Aldrich, R. W., Attali, B., Baggetta, A. M., Becirovic, E., Biel, M., Bill, R. M., Catterall, W. A., … Zhu, M. (2021). THE CONCISE GUIDE TO PHARMACOLOGY 2021/22: Ion channels. *British Journal of Pharmacology*, *178*(S1), S157–S245. https://doi.org/10.1111/bph.15539

Alexander, S. P. H., Roberts, R. E., Broughton, B. R. S., Sobey, C. G., George, C. H., Stanford, S. C., Cirino, G., Docherty, J. R., Giembycz, M. A., Hoyer, D., Insel, P. A., Izzo, A. A., Ji, Y., MacEwan, D. J., Mangum, J., Wonnacott, S., & Ahluwalia, A. (2018). Goals and practicalities of immunoblotting and immunohistochemistry: A guide for submission to the *British Journal of Pharmacology*. *British Journal of Pharmacology*, *175*(3), 407–411. https://doi.org/10.1111/bph.14112

Bang, S., Kim, K. Y., Yoo, S., Lee, S.-H., & Hwang, S. W. (2007). Transient receptor potential V2 expressed in sensory neurons is activated by probenecid. *Neuroscience Letters*, *425*(2), 120–125. https://doi.org/10.1016/j.neulet.2007.08.035

Bevan, S., Quallo, T., & Andersson, D. A. (2014). Trpv1. *Handbook of Experimental Pharmacology*, *222*, 207–245. https://doi.org/10.1007/978-3-642-54215-2_9

Bluhm, Y., Raudszus, R., Wagner, A., Urban, N., Schaefer, M., & Hill, K. (2022). Valdecoxib blocks rat TRPV2 channels. *European Journal of Pharmacology*, *915*, 174702. https://doi.org/10.1016/j.ejphar.2021.174702

Bobkov, D., & Semenova, S. (2022). Impact of lipid rafts on transient receptor potential channel activities. *Journal of Cellular Physiology*, Advance online publication, *237*, 2034–2044. https://doi.org/10.1002/jcp.30679

Bootman, M. D., Collins, T. J., Mackenzie, L., Roderick, H. L., Berridge, M. J., & Peppiatt, C. M. (2002). 2-Aminoethoxydiphenyl borate (2-APB) is a reliable blocker of store-operated Ca^{2+} entry but an inconsistent inhibitor of $InsP_3$-induced Ca^{2+} release. *FASEB Journal: Official Publication of the Federation of American Societies for Experimental Biology*, *16*(10), 1145–1150. https://doi.org/10.1096/fj.02-0037rev

Brundage, R. A., Fogarty, K. E., Tuft, R. A., & Fay, F. S. (1991). Calcium gradients underlying polarization and chemotaxis of eosinophils. *Science (New York, N.Y.)*, 254(5032), 703–706. https://doi.org/10.1126/science.1948048

Colton, C. K., & Zhu, M. X. (2007). 2-Aminoethoxydiphenyl borate as a common activator of TRPV1, TRPV2, and TRPV3 channels. *Handbook of Experimental Pharmacology*, 179, 173–187. https://doi.org/10.1007/978-3-540-34891-7_10

Curtis, M. J., Alexander, S. P. H., Cirino, G., George, C. H., Kendall, D. A., Insel, P. A., Izzo, A. A., Ji, Y., Panettieri, R. A., Patel, H. H., Sobey, C. G., Stanford, S. C., Stanley, P., Stefanska, B., Stephens, G. J., Teixeira, M. M., Vergnolle, N., & Ahluwalia, A. (2022). Planning experiments: Updated guidance on experimental design and analysis and their reporting III. *British Journal of Pharmacology*, 179, 3907–3913. https://doi.org/10.1111/bph.15868

Darby, M., Kuzmiski, J. B., Panenka, W., Feighan, D., & MacVicar, B. A. (2003). Atp released from astrocytes during swelling activates chloride channels. *Journal of Neurophysiology*, 89(4), 1870–1877. https://doi.org/10.1152/jn.00510.2002

Diena, T., Melani, R., Caci, E., Pedemonte, N., Sondo, E., Zegarra-Moran, O., & Galietta, L. J. V. (2007). Block of CFTR-dependent chloride currents by inhibitors of multidrug resistance-associated proteins. *European Journal of Pharmacology*, 560(2–3), 127–131. https://doi.org/10.1016/j.ejphar.2007.01.051

Edelstein, A., Amodaj, N., Hoover, K., Vale, R., & Stuurman, N. (2010). Computer control of microscopes using μManager. *Current Protocols in Molecular Biology*, 92(1), 14–20. https://doi.org/10.1002/0471142727.mb1420s92

Entin-Meer, M., & Keren, G. (2020). Potential roles in cardiac physiology and pathology of the cation channel TRPV2 expressed in cardiac cells and cardiac macrophages: A mini-review. *American Journal of Physiology. Heart and Circulatory Physiology*, 318(1), H181–H188. https://doi.org/10.1152/ajpheart.00491.2019

Froghi, S., Grant, C. R., Tandon, R., Quaglia, A., Davidson, B., & Fuller, B. (2021). New insights on the role of TRP channels in calcium signalling and immunomodulation: Review of pathways and implications for clinical practice. *Clinical Reviews in Allergy & Immunology*, 60(2), 271–292. https://doi.org/10.1007/s12016-020-08824-3

Frolov, R. V., & Singh, S. (2014). Celecoxib and ion channels: A story of unexpected discoveries. *European Journal of Pharmacology*, 730, 61–71. https://doi.org/10.1016/j.ejphar.2014.02.032

Grebert, C., Becq, F., & Vandebrouck, C. (2019). Focus on TRP channels in cystic fibrosis. *Cell Calcium*, 81, 29–37. https://doi.org/10.1016/j.ceca.2019.05.007

Heiner, I., Eisfeld, J., & Lückhoff, A. (2003). Role and regulation of TRP channels in neutrophil granulocytes. *Cell Calcium*, 33(5–6), 533–540. https://doi.org/10.1016/s0143-4160(03)00058-7

Iwata, Y., Ito, S., Wakabayashi, S., & Kitakaze, M. (2020). Trpv2 channel as a possible drug target for the treatment of heart failure. *Laboratory Investigation; a Journal of Technical Methods and Pathology*, 100(2), 207–217. https://doi.org/10.1038/s41374-019-0349-z

Jara-Oseguera, A., Simon, S. A., & Rosenbaum, T. (2008). Trpv1: On the road to pain relief. *Current Molecular Pharmacology*, 1(3), 255–269. https://doi.org/10.2174/1874467210801030255

Jordt, S.-E., Bautista, D. M., Chuang, H.-H., McKemy, D. D., Zygmunt, P. M., Högestätt, E. D., Meng, I. D., & Julius, D. (2004). Mustard oils and cannabinoids excite sensory nerve fibres through the TRP channel ANKTM1. *Nature*, 427(6971), 260–265. https://doi.org/10.1038/nature02282

Jung, N., Deckers, A., & Bräse, S. (2016). Molecule Archive of the Compound Platform. https://risources.dfg.de/detail/RI_00502_de.html

Kajiya, H., Okamoto, F., Nemoto, T., Kimachi, K., Toh-Goto, K., Nakayana, S., & Okabe, K. (2010). Rankl-induced TRPV2 expression regulates osteoclastogenesis via calcium oscillations. *Cell Calcium*, 48(5), 260–269. https://doi.org/10.1016/j.ceca.2010.09.010

Kogel, A., Kalwa, H., Urban, N., & Schaefer, M. (2019). Artifact-free objective-type multicolor total internal reflection fluorescence microscopy with light-emitting diode light sources—Part I. *Journal of Biophotonics*, 12(11), e201900033. https://doi.org/10.1002/jbio.201900033

Koyasu, S. (2010). Vanilloid flavor for a good appetite? *Nature Immunology*, 11(3), 187–189. https://doi.org/10.1038/ni0310-187

Lenz, J. C., Reusch, H. P., Albrecht, N., Schultz, G., & Schaefer, M. (2002). Ca^{2+}-controlled competitive diacylglycerol binding of protein kinase C isoenzymes in living cells. *Journal of Cell Biology*, 159(2), 291–301. https://doi.org/10.1083/jcb.200203048

Lévêque, M., Penna, A., le Trionnaire, S., Belleguic, C., Desrues, B., Brinchault, G., Jouneau, S., Lagadic-Gossmann, D., & Martin-Chouly, C. (2018). Phagocytosis depends on TRPV2-mediated calcium influx and requires TRPV2 in lipids rafts: Alteration in macrophages from patients with cystic fibrosis. *Scientific Reports*, 8(1), 4310. https://doi.org/10.1038/s41598-018-22558-5

Levin, R., Grinstein, S., & Canton, J. (2016). The life cycle of phagosomes: Formation, maturation, and resolution. *Immunological Reviews*, 273(1), 156–179. https://doi.org/10.1111/imr.12439

Lilley, E., Stanford, S. C., Kendall, D. E., Alexander, S. P., Cirino, G., Docherty, J. R., George, C. H., Insel, P. A., Izzo, A. A., Ji, Y., Panettieri, R. A., Sobey, C. G., Stefanska, B., Stephens, G., Teixeira, M., & Ahluwalia, A. (2020). ARRIVE 2.0 and the *British Journal of Pharmacology*: Updated guidance for 2020. *British Journal of Pharmacology*, 177(16), 3611–3616. https://doi.org/10.1111/bph.15178

Link, T. M., Park, U., Vonakis, B. M., Raben, D. M., Soloski, M. J., & Caterina, M. J. (2010). TRPV2 has a pivotal role in macrophage particle binding and phagocytosis. *Nature Immunology*, 11(3), 232–U7. https://doi.org/10.1038/ni.1842

Lock, J. T., Parker, I., & Smith, I. F. (2015). A comparison of fluorescent Ca^{2+} indicators for imaging local Ca^{2+} signals in cultured cells. *Cell Calcium*, 58(6), 638–648. https://doi.org/10.1016/j.ceca.2015.10.003

Magenau, A., Benzing, C., Proschogo, N., Don, A. S., Hejazi, L., Karunakaran, D., Jessup, W., & Gaus, K. (2011). Phagocytosis of IgG-coated polystyrene beads by macrophages induces and requires high membrane order. *Traffic (Copenhagen, Denmark)*, 12(12), 1730–1743. https://doi.org/10.1111/j.1600-0854.2011.01272.x

Missiaen, L., Callewaert, G., de Smedt, H., & Parys, J. B. (2001). 2-Aminoethoxydiphenyl borate affects the inositol 1,4,5-trisphosphate receptor, the intracellular Ca^{2+} pump and the non-specific Ca^{2+} leak from the non-mitochondrial Ca^{2+} stores in permeabilized A7r5 cells. *Cell Calcium*, 29(2), 111–116. https://doi.org/10.1054/ceca.2000.0163

Morera, F. J., Saravia, J., Pontigo, J. P., Vargas-Chacoff, L., Contreras, G. F., Pupo, A., Lorenzo, Y., Castillo, K., Tilegenova, C., Cuello, L. G., & Gonzalez, C. (2015). Voltage-dependent BK and Hv1 channels expressed in non-excitable tissues: New therapeutics opportunities as targets in human diseases. *Pharmacological Research*, 101, 56–64. https://doi.org/10.1016/j.phrs.2015.08.011

Nagasawa, M., Nakagawa, Y., Tanaka, S., & Kojima, I. (2007). Chemotactic peptide fMetLeuPhe induces translocation of the TRPV2 channel in macrophages. *Journal of Cellular Physiology*, 210(3), 692–702. https://doi.org/10.1002/jcp.20883

Nazıroğlu, M., Özgül, C., Çelik, Ö., Çiğ, B., & Sözbir, E. (2011). Aminoethoxydiphenyl borate and flufenamic acid inhibit Ca^{2+} influx through TRPM2 channels in rat dorsal root ganglion neurons activated by ADP-ribose and rotenone. *The Journal of Membrane Biology*, 241(2), 69–75. https://doi.org/10.1007/s00232-011-9363-9

Nilius, B., & Owsianik, G. (2011). The transient receptor potential family of ion channels. *Genome Biology*, 12(3), 218. https://doi.org/10.1186/gb-2011-12-3-218

Percie du Sert, N., Hurst, V., Ahluwalia, A., Alam, S., Avey, M. T., Baker, M., Browne, W. J., Clark, A., Cuthill, I. C., Dirnagl, U., Emerson, M., Garner, P., Holgate, S. T., Howells, D. W., Karp, N. A., Lazic, S. E., Lidster, K., MacCallum, C. J., Macleod, M., … Würbel, H. (2020). The

ARRIVE guidelines 2.0: Updated guidelines for reporting animal research. *PLoS Biology*, *18*(7), e3000410. https://doi.org/10.1371/journal.pbio.3000410

Qin, N., Neeper, M. P., Liu, Y., Hutchinson, T. L., Lubin, M. L., & Flores, C. M. (2008). Trpv2 is activated by cannabidiol and mediates CGRP release in cultured rat dorsal root ganglion neurons. *The Journal of Neuroscience: the Official Journal of the Society for Neuroscience*, *28*(24), 6231–6238. https://doi.org/10.1523/JNEUROSCI.0504-08.2008

Sághy, É., Szőke, É., Payrits, M., Helyes, Z., Börzsei, R., Erostyák, J., Jánosi, T. Z., Sétáló Jr, G., & Szolcsányi, J. (2015). Evidence for the role of lipid rafts and sphingomyelin in Ca^{2+}-gating of Transient Receptor Potential channels in trigeminal sensory neurons and peripheral nerve terminals. *Pharmacological Research*, *100*, 101–116. https://doi.org/10.1016/j.phrs.2015.07.028

Santoni, G., Farfariello, V., Liberati, S., Morelli, M. B., Nabissi, M., Santoni, M., & Amantini, C. (2013). The role of transient receptor potential vanilloid type-2 ion channels in innate and adaptive immune responses. *Frontiers in Immunology*, *4*, 34. https://doi.org/10.3389/fimmu.2013.00034

Sauer, K., & Jegla, T. J. (2006). Methods for identifying T cell activation modulating compounds. *Patent Application WO/2006/065613*.

Sawatani, T., Kaneko, Y. K., Doutsu, I., Ogawa, A., & Ishikawa, T. (2019). Trpv2 channels mediate insulin secretion induced by cell swelling in mouse pancreatic β-cells. *American Journal of Physiology. Cell Physiology*, *316*(3), C434–C443. https://doi.org/10.1152/ajpcell.00210.2017

Schneider, C. A., Rasband, W. S., & Eliceiri, K. W. (2012). NIH Image to ImageJ: 25 years of image analysis. *Nature Methods*, *9*(7), 671–675. https://doi.org/10.1038/nmeth.2089

Song, H. K., & Hwang, D. Y. (2017). Use of C57BL/6N mice on the variety of immunological researches. *Laboratory Animal Research*, *33*(2), 119–123. https://doi.org/10.5625/lar.2017.33.2.119

Spyra, S., Meisner, A., Schaefer, M., & Hill, K. (2017). Cox-2-selective inhibitors celecoxib and deracoxib modulate transient receptor potential vanilloid 3 channels. *British Journal of Pharmacology*, *174*(16), 2696–2705. https://doi.org/10.1111/bph.13893

Steele, E. M., & Steele, D. S. (2014). Automated detection and analysis of Ca^{2+} sparks in x-y image stacks using a thresholding algorithm implemented within the open-source image analysis platform ImageJ. *Biophysical Journal*, *106*(3), 566–576. https://doi.org/10.1016/j.bpj.2013.12.040

Svobodova, B., & Groschner, K. (2016). Mechanisms of lipid regulation and lipid gating in TRPC channels. *Cell Calcium*, *59*(6), 271–279. https://doi.org/10.1016/j.ceca.2016.03.012

Urban, N., Hill, K., Wang, L., Kuebler, W. M., & Schaefer, M. (2012). Novel pharmacological TRPC inhibitors block hypoxia-induced vasoconstriction. *Cell Calcium*, *51*(2), 194–206. https://doi.org/10.1016/j.ceca.2012.01.001

Urban, N., Wang, L., Kwiek, S., Rademann, J., Kuebler, W. M., & Schaefer, M. (2016). Identification and validation of larixyl acetate as a potent TRPC6 inhibitor. *Molecular Pharmacology*, *89*(1), 197–213. https://doi.org/10.1124/mol.115.100792

Wagner, M., Koester, H., Deffge, C., Weinert, S., Lauf, J., Francke, A., & Herold, J. (2014). Isolation and intravenous injection of murine bone marrow derived monocytes. *Journal of Visualized Experiments: JoVE*, Advance online publication, (94), e52347. https://doi.org/10.3791/52347

Wei, C., Wang, X., Chen, M., Ouyang, K., Song, L.-S., & Cheng, H. (2009). Calcium flickers steer cell migration. *Nature*, *457*(7231), 901–905. https://doi.org/10.1038/nature07577

Yamashiro, K., Sasano, T., Tojo, K., Namekata, I., Kurokawa, J., Sawada, N., Suganami, T., Kamei, Y., Tanaka, H., Tajima, N., Utsunomiya, K., Ogawa, Y., & Furukawa, T. (2010). Role of transient receptor potential vanilloid 2 in LPS-induced cytokine production in macrophages. *Biochemical and Biophysical Research Communications*, *398*(2), 284–289. https://doi.org/10.1016/j.bbrc.2010.06.082

Zhang, D., Spielmann, A., Wang, L., Ding, G., Huang, F., Gu, Q., & Schwarz, W. (2012). Mast-cell degranulation induced by physical stimuli involves the activation of transient-receptor-potential channel TRPV2. *Physiological Research*, *61*(1), 113–124. https://doi.org/10.33549/physiolres.932053

Zhang, X., Goncalves, R., & Mosser, D. M. (2008). The isolation and characterization of murine macrophages. *Current Protocols in Immunology*, Chapter 14, 14.1.1–14.1.14. https://doi.org/10.1002/0471142735.im1401s83

SUPPORTING INFORMATION

Additional supporting information can be found online in the Supporting Information section at the end of this article.